Available online at www.sciencedirect.com

ScienceDirect

Proceedings of the Combustion Institute 37 (2019) 3295–3302

Proceedings of the Combustion Institute

www.elsevier.com/locate/proci

Coupling of turbulence on the ignition of multicomponent sprays

Pavan B. Govindaraju [a,*], Thomas Jaravel [b], Matthias Ihme [a]

[a] *Department of Mechanical Engineering, Stanford University, Stanford, CA 94305, USA*
[b] *Center for Turbulence Research, Stanford, CA 94305, USA*

Received 28 November 2017; accepted 28 May 2018
Available online 18 July 2018

Abstract

This study examines the effect of turbulence on the ignition of multicomponent surrogate fuels and its role in modifying preferential evaporation in multiphase turbulent spray environments. To this end, two zero-dimensional droplet models are considered that are representative of asymptotic conditions of diffusion limit and the distillation limit are considered. The coupling between diffusion, evaporation and combustion is first identified using a scale analysis of 0D homogeneous batch reactor simulations. Subsequently, direct numerical simulations of homogeneously dispersed multicomponent droplets are performed for both droplet models, in decaying isotropic turbulence and at quiescent conditions to examine competing time scale effects arising from evaporation, ignition and turbulence. Results related to intra-droplet transport and effects of turbulence on autoignition and overall combustion are studied using an aviation fuel surrogate. Depending on the characteristic scale, it is shown that turbulence can couple through modulation of evaporation time or defer the ignition phase as a result of droplet cooling or gas-phase homogenization. Both preferential evaporation and turbulence are found to modify the ignition delay time, up to a factor of two. More importantly, identical droplet ignition behavior in homogeneous gas phase can imply fundamentally different combustion modes in heterogeneous environments.

Keywords: Droplets; Spray combustion; Multicomponent evaporation; Turbulence; Direct numerical simulation

1. Introduction

To enable the representation of transportation fuels containing a large number of compounds, surrogates are an established methodology [1], which involves selecting a set of species constituting the mixture along with finding the composition to closely match the physical and chemical properties of a particular fuel. The main complexity in emulating real-fuel behavior in practical applications arises from the strong interaction between the liquid and the gas phase. However, most studies have focused only on properties of the latter to construct surrogates.

Two-phase ignition behavior of liquid fuels has been studied using idealized systems to isolate chemical processes from other phenomena that affect combustion in real devices, as well as to make the problem computationally tractable using

* Corresponding author.
E-mail address: pavang@stanford.edu (P.B. Govindaraju).

https://doi.org/10.1016/j.proci.2018.05.166
1540-7489

detailed kinetic mechanisms. While experimental [2] and computational [3–5] studies have focused on the ignition behavior of single-component droplets, less attention has so far been devoted to the investigation of evaporation, ignition and combustion of multicomponent fuels in turbulent environments. In particular, the description of these fuels requires the consideration of liquid-phase diffusion, nonideal phase equilbrium, and extended chemical mechanisms for the description of multicomponent gas-phase chemistry. Recently, the role of preferential evaporation on the ignition of multicomponent fuels in homogeneous spray/air mixtures was demonstrated using an aviation fuel surrogate [6]. The treatment of the heterogeneous gas-phase, however, requires the use of multidimensional simulations and was performed only recently for multicomponent droplets [7]. However, these investigations focused on one-, two- and three-component surrogates in the early ignition stage and under quiescent ambient conditions. In contrast, turbulence effects on the ignition of sprays were so far only performed for single component fuels, with particular focus on the flame structure [8], low-temperature chemistry [9], droplet diameter and turbulent intensity [10] along with demonstrating phenomena, such as segregation and bifurcation [11].

The objective of this study is to investigate the coupling between the liquid and gas-phase in a heterogeneous turbulent environment and the effect of turbulence on the ignition of multicomponent droplets. The role of intra-droplet transport on the ignition of multicomponent fuel mixtures and the modification in their importance due to turbulence are hereby of particular interest. These effects are studied using two limiting conditions of zero-dimensional multicomponent evaporation, namely, the distillation and diffusion limits ([12], Pg. 95). The coupling between liquid phase and heterogeneous gas-phase is taken into account through direct numerical simulations of multicomponent combustion for varying droplet models and turbulent intensities in the gas-phase. The model formulation is presented in Section 2, where the physical and chemical aspects of the model is discussed. In Section 3, the model is applied to the analysis of autoignition of the 2nd-generation surrogate of the POSF 4658 Jet-A fuel [13]. A parametric study of effects of droplet diameter, overall equivalence ratio, evaporation models and the role of turbulence in modifying these effects is performed. The paper finishes by summarizing the main contributions of this work and offering conclusions in Section 4.

2. Model formulation

This section introduces the governing equations with a discussion about additional complexities introduced by multicomponent evaporation as compared to single-component fuels.

2.1. Gas-phase model

The conservation equations for mass, momentum, species and energy can be written in compact form as [12]

$$D_t\rho = \dot{S}_m, \tag{1a}$$

$$D_t(\rho u_i) = \dot{S}_{u_i} - \partial_i p + \partial_j \sigma_{ij}, \tag{1b}$$

$$D_t(\rho Y_k) = \partial_j\left(\rho D_k \partial_j Y_k\right) + \dot{\omega}_k + \dot{S}_m \delta_{k\{f\}}, \tag{1c}$$

$$\overline{c}_p D_t(\rho T) = \partial_j\left(\lambda \partial_j T\right) + \dot{\omega}_T + \dot{S}_T, \tag{1d}$$

where $D_t = \partial_t + u_i\partial_i$, $\partial_i = \partial/\partial_{x_i}$, ρ is the gas density, u_i is the gas velocity, p is the pressure, T is the gas temperature, Y_k is the species mass fraction of the k^{th} species. $\dot{S}_m$, $\dot{S}_{u_i}$ and $\dot{S}_T$ are the source terms due to mass evaporation, drag and heat transfer, respectively; $\delta_{k\{f\}}$ is the Kronecker delta function equal to 1 if k belongs to the liquid species ensemble $\{f\}$ and zero otherwise; σ_{ij} is the viscous stress tensor, D_k is the mixture-diffusivity of species k, $\dot{\omega}_k$ is the production rate of species k, λ is the thermal conductivity, c_p is the mixture-averaged heat capacity and $\dot{\omega}_T = -\sum_{k=1}^{N_s} h_k\dot{\omega}_k$ is the heat release rate.

2.2. Liquid-phase model

The dispersed liquid droplets are described by a Lagrangian point-particle method [14], which is commonly used for turbulent spray combustion simulations [15]. In contrast with the continuous thermodynamic (CT) approach [16], a discrete multicomponent liquid description is used to resolve individual species mass fractions as a function of time. Fickian diffusion is used due to the large number of species along with neglecting the Soret and Dufour effects. The governing equations for each droplet can be written as [14]

$$d_t x_{d,i} = u_{d,i}, \tag{2a}$$

$$d_t u_{d,i} = f_1\tau_d^{-1}\left(u_{i@d} - u_{d,i}\right), \tag{2b}$$

$$d_t m_{d,k} = \dot{m}_{ev,k}, \tag{2c}$$

$$d_t T_d = \frac{Nu}{3Pr}\frac{c_p}{c_L}\frac{f_2}{\tau_d}\left(T_{@d} - T_d\right) + \frac{\sum_{k\in\{f\}}\dot{m}_{ev,k}L_{v,k}}{m_d c_L}, \tag{2d}$$

where $x_{d,i}$ and $u_{d,i}$ are the droplet position and velocity component, respectively. τ_d is the droplet relaxation time given by $\tau_d = \rho_l d^2/(18\mu_g)$, with ρ_l the liquid density, d the droplet diameter, and μ_g the dynamic viscosity of the gas-phase mixture.

$u_{i@d}$ represents the gas velocity at the droplet location, $m_{d,k}$ is the mass of species k, T_d is the droplet temperature and $T_{@d}$ is the gas temperature at the droplet location. Nu and Pr are the Nusselt and Prandtl number, respectively. $L_{v,k}$ is the latent heat of vaporization of species k, m_d is the droplet mass and c_L is the averaged liquid heat capacity. f_1 accounts for deviations from Stokes drag and f_2 represents the Nusselt number correction due to evaporation, and these corrections are discussed in [14].

To examine effects of preferential evaporation, two limiting conditions of intra-droplet diffusion are considered [12, Pg. 95], which are characterized by the surface composition. For fast-evaporating droplets, particularly in combustion, the evaporation rate is faster than internal transport, giving rise to the *diffusion limit*, and under the limit of infinite Peclet number, the mass-flux fraction of a given species off the surface is equal to the initial liquid-phase mass fraction, since boundary layer effects are negligible [17]. The surface adjusts appropriately based on the volatility to maintain the same proportion of components in the droplet. Mixture-averaged transport properties are to be used in this model as the individual species transport does not dictate evaporation in this limit. On the contrary, the *distillation limit* model represents rapid internal mixing, either due to high liquid diffusion or circulation and the surface composition is the same as the entire droplet. The compounds evaporate sequentially according to their volatility [18]. In summary, the evaporation source terms for the diffusion-limit $\dot{m}_{ev,k,dif}$ and the distillation-limit $\dot{m}_{ev,k,dil}$ can be written as [19, Pg. 183]

$$\dot{m}_{ev,k,dif} = -\frac{\overline{Sh}}{3\overline{Sc}}\frac{m_d}{\tau_d}\ln(1+B_M)Y_{l,k}, \tag{3a}$$

$$\dot{m}_{ev,k,dil} = -\frac{Sh_k}{3Sc_k}\frac{m_d}{\tau_d}\ln(1+B_{M,k}), \tag{3b}$$

where $Sh_k = 2 + 0.552\,Re^{1/2}$ and $Sc_k{}^{1/3}$ are the Sherwood number and the Schmidt number for species k and $\overline{Sh}$ and $\overline{Sc}$ are their mixture-averaged counterparts, respectively. $B_{M,k}$ is the mass-transfer number of species k [20] evaluated from the cumulative Spalding mass-transfer number, written as

$$B_M = \frac{\sum_{k\in\{f\}}(Y_{sat,k} - Y_k)}{1 - \sum_{k\in\{f\}} Y_{sat,k}}.$$

The cell-averaged value is used for Y_k along with the 1/3-rule for evaluating thermophysical properties. The droplet model assumes that Y_k is based on the value at infinity; in multicomponent spray situations, approximations for Y_k is a subject of ongoing research. Current methods such as region of influence [21] utilize 2–5d_0 as the radius of averaging, and the current work also uses similar cell sizes. The boundary condition at the phase-interface is determined using the ideal Raoult's law as the fuel compounds are non-polar. The Sherwood and Schmidt numbers are evaluated at reference conditions using the 1/3-rule and mixing rules for viscosity, thermal conductivity and species diffusivity [22]. The thermodynamic and transport properties of the fuel are obtained using a group contribution approach [23].

2.3. Surrogate formulation and chemical mechanism

This study focuses on the conventional Jet-A POSF 4658 fuel blend, for which an extensive set of experimental data is available. An experimental approach for the formulation of the surrogate representation of transportation fuels was developed and used by Dooley et al. [24]. The final composition obtained after matching target properties is n-dodecane, iso-octane, 1,3,5-trimethylbenzene and n-propylbenzene in molar fractions of 0.404, 0.295, 0.073 and 0.228, respectively. This surrogate composition is considered throughout this study.

The kinetic mechanism used for the description of the gas-phase chemistry is derived from the lumped model by Ranzi et al. [25] and a skeletal reduction procedure [26] is applied to obtain a final mechanism of 181 species and 4089 reactions [6], required to capture low-temperature ignition, whose effects will be shown to be particularly modified by turbulence.

2.4. Numerical solver

The governing equations are solved using the structured NGA code [27]. A QUICK scheme is used for the discretization of the scalar advection operators, and a second-order central scheme is used for solving the momentum and pressure equations. The chemical source term and analytical Jacobian are efficiently evaluated using `pyJac` [28], making the problem computationally tractable as it now scales linearly with the number of species, as opposed to having quadratic complexity when a finite-difference approximation for the Jacobian is used. Also, the large and stiff nature of the chemical mechanism necessitates the use of a the specialized nonlinear solver `BzzNls` [29].

3. Ignition of multicomponent sprays

This section discusses the ignition of multicomponent sprays in quiescent and turbulent flow environments. Effect of droplet diameter, global equivalence ratio and the role of preferential evaporation and turbulence are the particular topics of discussion.

3.1. Scale analysis

Isolated droplet simulations were performed for the 2nd generation POSF surrogate as a function of droplet diameter d_0 and global equivalence ratio

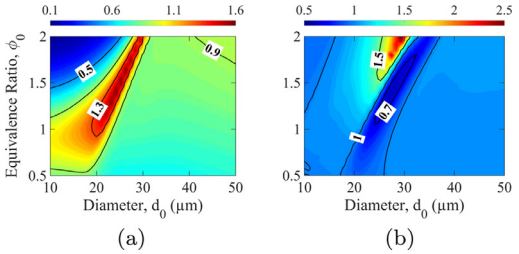

Fig. 1. Time scale analysis of 2nd generation POSF 4658 surrogate [13] droplet combustion, showing a) $(\tau_{evap} + \tau_{pv,ign})/\tau_{ign,\,dif}$ for the diffusion-limited model and b) $\tau_{ign,\,dil}/\tau_{ign,\,dif}$ at $p_0 = 10$ bar and $T_0 = 833$ K in a quiescent environment.

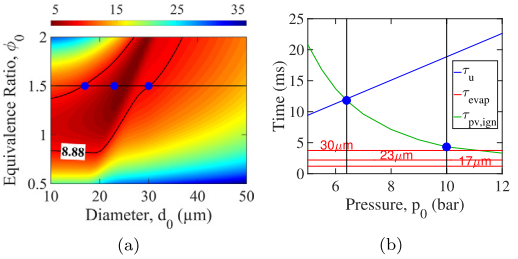

Fig. 2. a) Autoignition delay time [ms] for isolated POSF 4658 surrogate droplet using diffusion-limit model at $p_0 = 10$ bar and $T_0 = 833$ K. The blue circles indicate the conditions for the DNS simulations b) Time-scale of the eddy-turnover time (τ_u), droplet evaporation time (τ_{evap}) and pre-vaporized autoignition time ($\tau_{pv,\,ign}$) as a function of pressure. (For interpretation of the references to color in this figure legend, the reader is referred to the web version of this article.)

ϕ_0 at ambient temperature $T_0 = 833$ K and $p_0 = \{6.4, 10\}$ bar, relevant to gas turbine settings, in a constant-volume setting. The idealized picture for spray combustion [30, Pg. 49] considers that the ignition delay of a droplet cloud results from sequential processes of evaporation and gaseous autoignition, so that the total ignition time (τ_{ign}) can be approximated as $\tau_{ign} \simeq \tau_{evap} + \tau_{pv,ign}$, where τ_{evap} is the evaporation time, $\tau_{pv,\,ign}$ is the autoignition time of the pre-vaporized mixture.

However, depending on quenching conditions, droplet diameter and equivalence ratio, the total time to ignition differs from the idealized representations. The cooling effect due to droplet evaporation delays the vapor autoignition time and for small droplets, at higher equivalence ratios, immediate fuel availability causes ignition before the droplet completely evaporates [6], thus causing the autoignition time to differ from the ideal description. The total time is different based on the intra-droplet diffusion and is denoted by $\tau_{ign,\,dil}$ for the distillation-limit and $\tau_{ign,\,dif}$ for the diffusion-limit. Figure 1(a) shows the autoignition time for an isolated droplet as a function of droplet diameter and equivalence ratio using the diffusion-limit model, and is found to significantly deviate from the ideal description. Also, for particular equivalence ratio and droplet diameter combinations, the ratio of ignition times between the two droplet models, shown in Fig. 1(b), differs by as much as a factor of two, and thus emphasizes the effect of preferential evaporation.

Relevant cases for direct numerical simulations to examine effects of heterogeneous gas-phase, group combustion and turbulence are identified. For this, simulation parameters are selected with the intent to demonstrate the role of preferential evaporation, and the interaction between evaporation, turbulence and autoignition in a pairwise fashion along with being relevant to gas turbine operating conditions. The chosen configuration of uniformly distributed droplets in decaying homogeneous turbulence is based on previous studies of auto-ignition [9]. The computational domain consists of a cubic box of length $L = 12.0$ mm, discretized using 256 grid points in each direction, corresponding to a spatial resolution of 47 μm. The turbulent velocity is initialized using a Passot–Pouquet energy spectrum [31] with an integral length scale $L_u = L/6$. The initial turbulent velocity fluctuations are chosen to ensure a Kolmogorov length scale of $\eta_K = 60$ μm, which is resolved using the current resolution. Also, note that the droplet size and mass loading ratio is maintained to be low enough to not violate the Lagrangian point-particle approximation [32, Pg. 286]. The corresponding timescales are $\tau_u = L_u/u' = 19$ ms for the eddy turnover time and $\tau_K = 0.3$ ms for the Kolmogorov timescale. The separation parameter based on these numbers is $\mathcal{O}(10)$ so that the spray burning behavior falls in the group combustion regime [33].

Figure 2(a) illustrates the autoignition delay time for an isolated droplet using the diffusion-limit model, as it is a better representation of combustion settings [12, Pg. 95]. From this, the first set of cases is selected to maximize the role of preferential evaporation while maintaining a low autoignition time. This corresponds to $d_0 = 23$ ms, $\phi_0 = 1.5$ and a pressure of $p_0 = 10$ bar. Note that the distillation-limit model is also evaluated for comparison at this point. This configuration corresponds to an evaporation time of $\tau_{evap} = 2.3$ ms and a gas autoignition time of 4.3 ms. The next set of cases are based on the same global equivalence ratio, thus maintaining the gas-phase ignition time and cooling effect. To study the coupling of evaporation with turbulence, two droplet diameters, 17 and 30 μm are chosen as they have the same isolated droplet autoignition time, as shown in Fig. 2(a). The autoignition time however, is still quite fast compared to the eddy turnover time, as shown in Fig. 2(b), and these can be made identical by reducing the ambient pressure p_0 to 6.4 bar. The DNS configurations used in this study are summarized in Table 1, with each corre-

Table 1
Summary of spray and turbulence properties used in the DNS study. $T_0 = 833K$ for all cases.

#	d_0 (μm)	p_0 (bar)	u' (m/s)	$\dot{m}_{ev,k}$ (Eq.)	τ_{evap} (ms)	$\tau_{pv,\ ign}$ (ms)	τ_u (ms)
1	23	10	1.5	(3a)	2.3	4.3	19
2	23	10	1.5	(3b)	2.6	4.3	19
3	17	10	1.5	(3a)	1.2	4.3	19
4	30	10	1.5	(3a)	3.1	4.3	19
5	23	6.4	2.6	(3a)	2.1	11.2	11.2

sponding to two simulations; using quiescent or decaying isotropic turbulent environment as ambient, respectively.

3.2. Spray autoignition and preferential evaporation

This subsection focuses on the impact of preferential evaporation using the first set of simulations (Cases 1–2) from Table 1. For these cases, significant coupling is expected between preferential evaporation and ignition, because evaporation and ignition time scales are of the same order. To understand the spray ignition process, volume-averaged mean quantities are first extracted and compared in Fig. 3. Instantaneous flow field results at selected time instances (marked in Fig. 3(a)) are shown in Fig. 4. The mean temperature evolution (Fig. 3(a)) shows that the ignition process can be decomposed into different phases. At first, the gas temperature drops because of the energy transfer to the droplets for evaporation and the initial cooling phase is similar for both evaporation models. This is supported by the mass-weighted mean droplet temperature, illustrated in Fig. 3(b), which shows that both models are identical during the droplet heating phase. However, the distillation model reaches a higher final temperature as this model requires the boiling point of each component to be reached for complete evaporation. Figure 4a shows an instantaneous flow field at this early evaporation stage and indicates that significant temperature reduction occurs in the vicinity of the droplets, demonstrating the importance of turbulent motion in enhancing the evaporation. The evaporation leads to transfer of fuel compounds (Fig. 3(c) and 3(f)) to the gas phase. The process is strongly heterogeneous, with typical scales on the order of the droplet spacing, as shown by the n-dodecane field in Fig. 4a. Once the evaporation is completed ($t \simeq 2.2$ ms), the mean temperature plateaus for the turbulent cases. Due to turbulent mixing, heterogeneities in the gas-phase are transformed into larger, coherent pockets, where the high mass fraction of fuel correlates with low temperature levels, as shown in Fig. 4b. This is also evident from the variance of the n-dodecane mass fraction in Fig. 3(d), which peaks at the end of the evaporation followed by a decrease

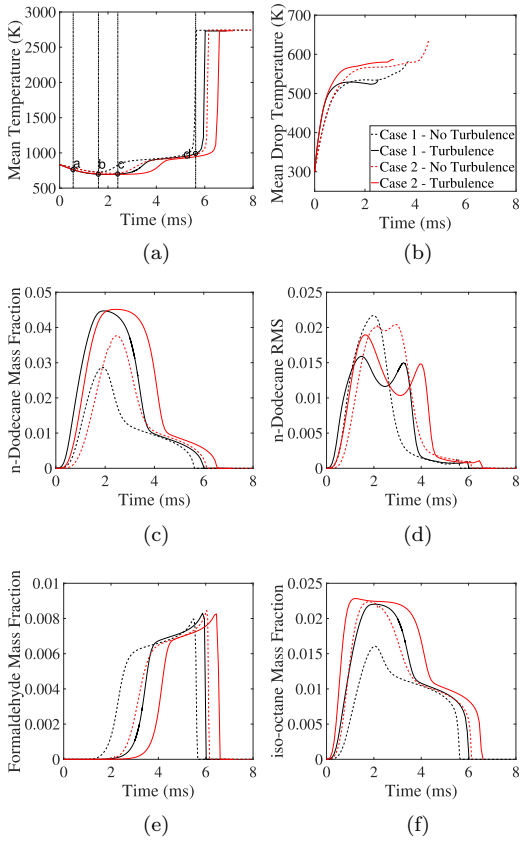

Fig. 3. Temporal evolution of volume-averaged quantities. Comparison between DNS data for the diffusion-limit model (Case 1) and distillation-limit (Case 2) at $p_0 = 10$ bar, $\phi_0 = 1.5$ and $d_0 = 23$ μm for quiescent and turbulent ambient conditions.

under turbulence, whereas it remains high for the non-turbulent cases.

Regarding the fuel compounds, iso-octane preferentially evaporates significantly faster for the distillation-limited model (Fig. 3(e)). However, this evaporation model predicts a lower evaporation rate for the most reactive species, namely, n-dodecane. Following the temperature plateau phase, observed for turbulent cases, some isolated pockets start to pre-ignite, as indicated by the localized formation of regions of high CH_2O mass fraction in Fig. 4c, with higher temperature and lower fuel concentration. This isolated phenomena then extends to the rest of the domain around $t = 3.4$ ms for the turbulent cases, with an increase in the mean temperature (Fig. 3(a)). For non-turbulent cases, the situation is appreciably different and the pre-ignition phase is triggered before the end of the evaporation phase, leading to a coupled evaporation-ignition regime. The low-temperature preignition is characterized by a drop in the mass

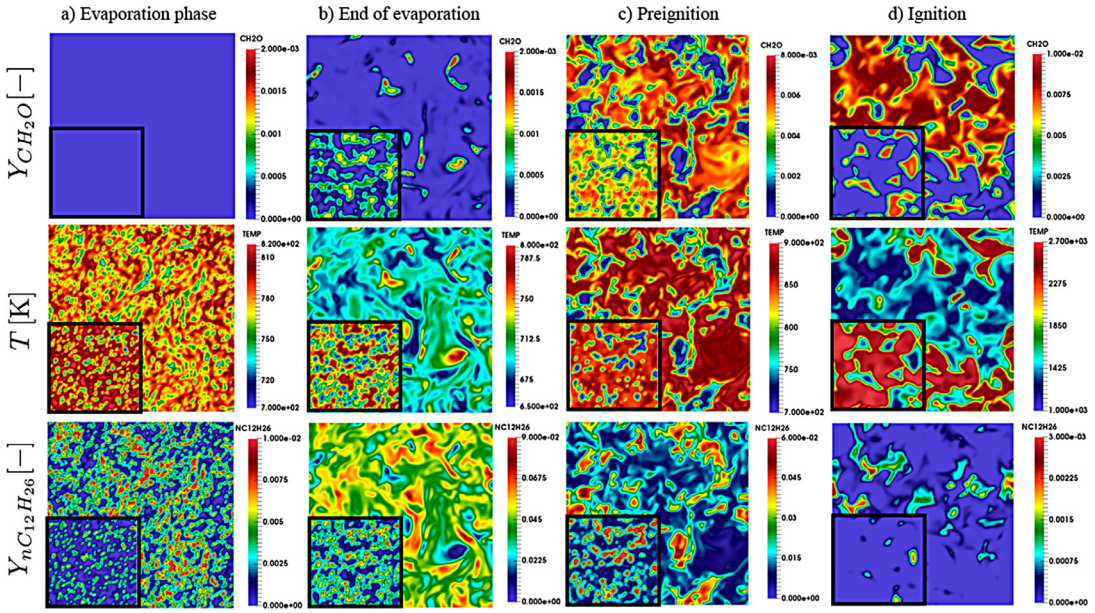

Fig. 4. Two dimensional fields of (top) CH_2O, (middle) temperature and (bottom) n-$C_{12}H_{26}$ for four different time instances indicated in Fig. 3, corresponding, respectively, to (a) evaporation phase, (b) end of the evaporation, (c) preignition and (d) ignition for Case 2 with an insert showing the same case without turbulence.

fraction of fuel compounds (Fig. 3(c) and 3(f)) and the formation of CH_2O radicals (Fig. 3(e)). Figure 4c shows that the preignition is highly heterogeneous, some pockets igniting much later than others, which results in a second peak of n-dodecane fluctuation (Fig. 3(d)) during the preignition phase for the turbulent cases. After preignition, the mixing continues to homogenize the mixture and complete ignition occurs around $t = 6$ ms. Figure 4d shows that the ignition structure is less dense compared to the pre-ignition kernels, particularly for the non-turbulent simulation, thus highlighting the importance of turbulent mixing in flame propagation. Despite being moderate, preferential evaporation effects observed for the distillation-limit evaporation model are sufficient to delay the preignition by 10% for the turbulent case compared to the diffusion-limit model, which is a consequence of the fact that the evaporation rates of the most reactive fuel compounds are slower in this case. The delay in preignition represents half of the time leading to it after evaporation and primarily contributes to the difference in autoignition delay time.

3.3. *Evaporation-turbulence interaction*

We proceed by discussing the role of turbulence on the cases with droplet diameter $d_0 = 17$ μm and 30 μm, which have identical 0D autoignition time, as shown in Fig. 2(a). Heterogeneous gas-phase effects along with the role of turbulence are shown to be evident as they lead to dissimilar profiles in several statistical quantities for the cases under consideration.

Relevant results from the second set of cases (Cases 3–4) in Table 1 are shown in Fig. 5. Both droplet diameters share the same 0D autoignition time of 8.88 ms. However, from the instant of reduction in $\langle Y_{CH_2O} \rangle$, shown in Fig. 5(a), and the rise in the mean temperature of the gas phase, shown in Fig. 5(b), ignition is observed to occur well in advance compared to the 0D time, emphasizing the importance of heterogeneous gas-phase effects and not just turbulence. The mixture generated from the smaller droplets takes longer to ignite and turbulence only increases the difference in ignition time. Figure 5(c) shows the mass fraction variance of n-dodecane and the mode of combustion is found to be different in both cases, with the smaller droplet showing distinct evaporation and pre-ignition phase, while the droplets having larger diameters demonstrate coupled behavior. Note that the larger diameter does not present a distinct pre-ignition phase for the non-turbulent case, also shown in Fig. 5(b), where the mean temperature continuously increases after the cooling phase. Turbulent gas-phase effects lead to different mass-weighted droplet temperature profiles, shown in Fig. 5(d), with changes in diameter, given that 0D isolated droplets have identical temperature profiles. The higher temperature for the larger droplets is due to the coupling with combustion, leading to higher local ambient temperatures.

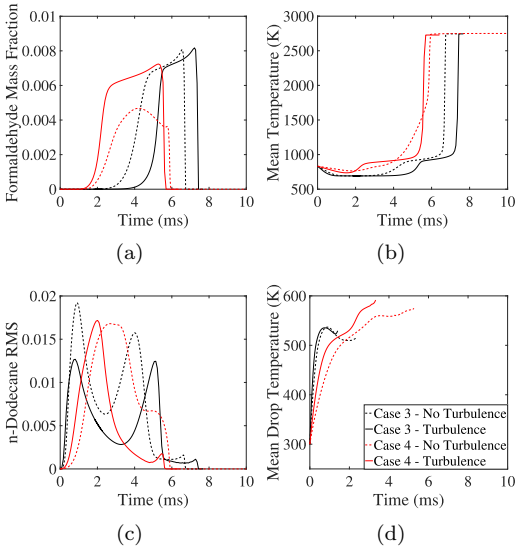

Fig. 5. Temporal evolution of volume-averaged quantities. Comparison between DNS data for the diffusion-limit model at $p_0 = 10$ bar, $\phi_0 = 1.5$, $T_0 = 833$ K and $d_0 = \{17\ \mu m, 30\ \mu m\}$ (Case 3 and 4) for quiescent (dashed) and turbulent (solid) ambient conditions.

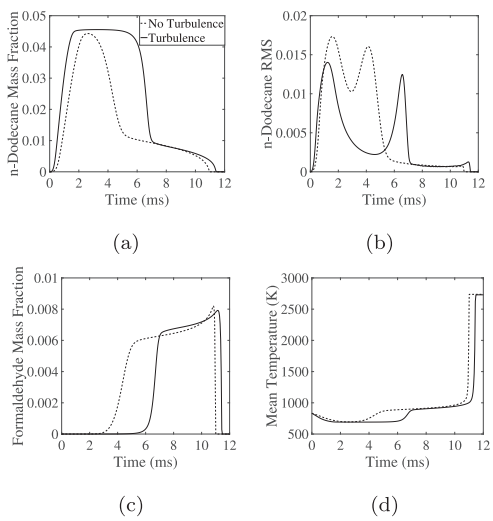

Fig. 6. Comparison between DNS data for the diffusion-limit model (Case 5) at $p_0 = 6.4$ bar, $d_0 = 23\ \mu m$, $\phi_0 = 1.5$ and $T_0 = 833$ K for quiescent and turbulent ambient conditions.

Turbulence leads to faster evaporation and creates inhomogenities in the local temperature fields, thus separating the droplet temperature profiles.

3.4. Autoignition-turbulence interaction

The last case (Case 5) in Table 1 represents the interaction between autoignition and turbulence, given that the eddy-turnover time (τ_u) and autoignition time of the prevaporized fuel ($\tau_{pv,\ ign}$) are the same, well separated from the evaporation time (τ_{evap}).

Figure 6 shows a comparison between the turbulent and non-turbulent simulations at $p_0 = 6.4$ bar, presented in Table 1. The effect of turbulence can be observed in the mean mass fraction plot of n-dodecane, shown in Fig. 6(a). Note that other fuel components follow the same trend, given that the diffusion model is used. The faster evaporation due to advected droplets in the turbulent environment leads to peak mass fractions being reached earlier. However, the onset of low-temperature ignition (second peak in Fig. 6(b)) is quicker in the non-turbulent case due to mixture inhomogenities leading to certain locations being favorable. This is more evident in Fig. 6(b), where the first peak corresponds to the inhomogenity arising from evaporation and the second peak is from the onset of low-temperature combustion, as discussed in Section 3.2. Note that the final ignition occurs at nearly homogeneous conditions for both cases. Figure 6(c) and 6(d) illustrate the onset of low-temperature combustion, showing that the homogenizing effect of turbulence delays low-temperature ignition by a factor of two. The low pressure slows down the chemical time scale and thus, the difference in the resulting pre-ignition time is more evident in this case, as opposed to Fig. 5(b), where the smaller droplets showed similar behavior. Trends in second-stage ignition are dictated by a number of competing factors, namely, reactant availability along with formation and propagation of the ignition kernel [9]; turbulence can either attenuate or amplify ignition, as seen in the difference in order of ignition for the two cases in Fig. 5.

4. Conclusions

This work studied the effect of turbulence on the ignition of multicomponent surrogate fuels. To this purpose, two zero-dimensional droplet models that represent limiting conditions of intra-droplet transport are chosen for the 2nd-generation surrogate of a POSF 4658 Jet-A fuel and a validated skeletal mechanism (181 species, 4089 reactions) was used to describe the gas-phase chemistry.

A timescale analysis was performed to identify coupling between diffusion, evaporation, combustion and turbulence. The importance of multicomponent evaporation effects in a heterogeneous environment is shown. This guided direct numerical simulations to identify the role of turbulence on preferential evaporation effects, droplet vaporization and autoignition.

Simulation results show that turbulence significantly enhances fuel vaporization and preferential evaporation effects are evident from the fundamen-

tally different combustion behavior between both evaporation models. DNS analysis highlights the impact of cooling around droplets, homogenizing effects by turbulence and the merging of ignition kernels. The effect of droplet diameter is emphasized by considering two cases which have identical 0D ignition time but show contrasting combustion behavior. The interaction between chemical and turbulent time scales is studied using a lower pressure, which highlights the effect of turbulence on low-temperature ignition.

DNS studies considered in this work are limited by a restricted range of feasible time scales, due to approximations in the treatment of multiphase flows and computational cost to resolve the flame structure. Diffusion models better capture the timescales involved in practical ignition settings even under turbulent settings.

Acknowledgments

The authors gratefully acknowledge financial support through NASA with award NNX15AV04A. Resources supporting this work were provided by the NASA High-End Computing (HEC) Program through the NASA Advanced Supercomputing (NAS) Division at Ames Research Center.

References

[1] T.J. Edwards, L.Q. Maurice, *J. Propul. Power* 17 (2) (2001) 461–466.
[2] M. Tanabe, T. Bolik, C. Eigenbrod, H.J. Rath, J. Sato, M. Kono, *Symp. (Int.) Combust.* 26 (1) (1996) 1637–1643.
[3] A. Cuoci, M. Mehl, G. Buzzi-Ferraris, T. Faravelli, D. Manca, E. Ranzi, *Combust. Flame* 143 (3) (2005) 211–226.
[4] O. Moriue, M. Mikami, N. Kojima, C. Eigenbrod, *Proc. Combust. Inst.* 30 (2) (2005) 1973–1980.
[5] T.I. Farouk, F.L. Dryer, *Combust. Flame* 161 (2) (2014) 565–581.
[6] A. Stagni, L. Esclapez, P. Govindaraju, A. Cuoci, T. Faravelli, M. Ihme, *Proc. Combust. Inst.* 36 (2) (2017) 2483–2491.
[7] T. Kitano, J. Nishio, R. Kurose, S. Komori, *Fuel* 136 (2014) 219–225.
[8] K. Luo, H. Pitsch, M.G. Pai, O. Desjardins, *Proc. Combust. Inst.* 33 (2) (2011) 2143–2152.
[9] G. Borghesi, E. Mastorakos, R.S. Cant, *Combust. Flame* 160 (7) (2013) 1254–1275.
[10] H. Wang, K. Luo, J. Fan, *Fuel* 121 (2014) 311–318.
[11] A. Vié, B. Franzelli, Y. Gao, T. Lu, H. Wang, M. Ihme, *Proc. Combust. Inst.* 35 (2) (2015) 1675–1683.
[12] W.A. Sirignano, *Fluid Dynamics and Transport of Droplets and Sprays*, Cambridge University Press, 2010.
[13] S. Dooley, S.H. Won, J. Heyne, et al., *Combust. Flame* 159 (4) (2012) 1444–1466.
[14] R.S. Miller, K. Harstad, J. Bellan, *Int. J. Multiph. Flow* 24 (6) (1998) 1025–1055.
[15] P. Jenny, D. Roekaerts, N. Beishuizen, *Prog. Energy Combust. Sci.* 38 (6) (2012) 846–887.
[16] J. Tamim, W.L.H. Hallett, *Chem. Eng. Sci.* 50 (18) (1995) 2933–2942.
[17] B.D. Shaw, *Combust. Flame* 81 (3–4) (1990) 277–288.
[18] A. Makino, C.K. Law, *Combust. Flame* 73 (3) (1988) 331–336.
[19] L. Esclapez, P. Govindaraju, M. Ihme, *CTR Center for Turbulence Research Annu.Res. Briefs* (2016) 181–192.
[20] C. Wang, A.M. Dean, H. Zhu, R.J. Kee, *Combust. Flame* 160 (2) (2013) 265–275.
[21] S.S. Sazhin, A.E. Elwardany, P.A. Krutitskii, et al., *Int. J. Therm. Sci.* 50 (7) (2011) 1164–1180.
[22] L.C. Chow, J.N. Chung, *Int. J. Heat Mass Transf.* 26 (3) (1983) 373–380.
[23] P.B. Govindaraju, M. Ihme, *Int. J. Heat Mass Transf.* 102 (2016) 833–845.
[24] S. Dooley, S.H. Won, M. Chaos, et al., *Combust. Flame* 157 (12) (2010) 2333–2339.
[25] E. Ranzi, A. Frassoldati, R. Grana, et al., *Prog. Energy Combust. Sci.* 38 (4) (2012) 468–501.
[26] A. Stagni, A. Frassoldati, A. Cuoci, T. Faravelli, E. Ranzi, *Combust. Flame* 163 (2016) 382–393.
[27] O. Desjardins, G. Blanquart, G. Balarac, H. Pitsch, *J. Comput. Phys.* 227 (15) (2008) 7125–7159.
[28] K.E. Niemeyer, N.J. Curtis, C.-J. Sung, *Comput. Phys. Commun.* 215 (2017) 188–203.
[29] D. Manca, G. Buzzi-Ferraris, A. Cuoci, A. Frassoldati, *Comput. Chem. Eng.* 33 (10) (2009) 1727–1734.
[30] A.H. Lefebvre, *Gas Turbine Combustion*, CRC Press, 1998.
[31] T. Passot, A. Pouquet, *J. Fluid Mech.* 181 (1987) 441–466.
[32] A. Prosperetti, G. Tryggvason, *Computational Methods for Multiphase Flow*, Cambridge University Press, 2009.
[33] J. Reveillon, L. Vervisch, *J. Fluid Mech.* 537 (2005) 317–347.